# Numerical Simulations Confirm Wave-Induced Shear Mixing in Stellar Interiors

A. Varghese,[1] R.P. Ratnasingam,[2] L. Ramírez-Galeano,[3] S. Mathis,[1] and T.M. Rogers[2,4]

[1] *Université Paris-Saclay, Université Paris Cité, CEA, CNRS, AIM, F-91191, Gif-sur-Yvette, France*
[2] *Newcastle University, Newcastle Upon Tyne, United Kingdom*
[3] *University of Geneva, Geneva, Switzerland*
[4] *Planetary Science Institute, Tucson, AZ, USA*

## ABSTRACT

Internal Gravity Waves (IGWs) are thought to cause mixing in stellar interiors, a process that has been widely studied both theoretically and numerically. Our aim is to determine the physical mechanism responsible for the wave-induced mixing in stellar interiors. We compare the mixing profiles obtained from two-dimensional (2D) equatorial hydrodynamical and tracer particle simulations with theoretical predictions from R. J. Garcia Lopez & H. C. Spruit (1991) and J. P. Zahn (1992) on wave mixing due to wave-induced shear turbulence. Our results show that, despite not satisfying the vertical shear instability threshold, the mixing profiles from the simulations agree remarkably well with the theoretical predictions of both prescriptions, strongly suggesting that shear from IGWs plays an important role in mixing even at low shear rates. This agreement remains robust across different stellar masses, ages, rotation and simulation parameters. This provides an important step in providing realistic parameterisations for wave mixing in stellar structure and evolution models.

## 1. INTRODUCTION

Mixing processes in stellar radiative interiors affects the distribution of chemicals, influencing the lifetime, evolution and the final stages of stars (A. Maeder 2009). Constraining this internal mixing is necessary for the accurate modelling of stellar structure and evolution. This has been an ongoing challenge for decades and various mixing mechanisms have been proposed as the source of additional mixing in stars to improve stellar evolution models (S. Mathis 2013; C. Aerts et al. 2019). Our understanding of stellar interiors has improved significantly with the recent advances in asteroseismology, which have provided new insights into properties such as internal rotation and mixing from the core to the surface (C. Aerts & A. Tkachenko 2024). Among the various internal processes proposed to cause mixing, Internal Gravity Waves (IGWs) are a leading candidate. These waves were already known to play a major role in the transport of energy and momentum in the Earth's atmosphere and oceans (J. R. Holton 1982; M. J. Alexander et al. 2010).

In stars, IGWs are thought to transport angular momentum (E. Schatzman 1993; J. P. Zahn et al. 1997; P. Kumar et al. 1999) and chemicals (W. H. Press 1981; R. J. Garcia Lopez & H. C. Spruit 1991; S. Talon &

Email: ashlin.varghese@cea.fr

C. Charbonnel 2005). This process has been widely explored theoretically for the last $\sim$ 40 years. R. J. Garcia Lopez & H. C. Spruit (1991) proposed that the shear induced by IGW could produce the weak turbulence needed to cause mixing, that could possibly explain the Li depletion in the Sun and F-type stars. Their model assumes a Kolmogorov spectrum for the turbulent eddies at the convective-radiative boundary and an incoherent distribution of convective eddies exciting monochromatic waves that propagate into the stable layer. They argued that in a steady flow, the vertical shear induced by IGWs can lead to small-scale turbulence capable of driving mixing, with a IGW diffusion coefficient that scales with the square of the wave amplitude, determined by the Richardson number and thermal diffusion. J. P. Zahn (1992) estimated the diffusion coefficient for shear-induced mixing in stably stratified flows, based on a detailed analysis of anisotropic turbulence focusing on large scale shears. Although not specific to wave-driven flows, J. P. Zahn (1992)'s prescription similarly assumes that the largest eddies dominate vertical transport and retrieve a diffusion coefficient similar to that of R. J. Garcia Lopez & H. C. Spruit (1991).

Apart from turbulence, W. H. Press (1981) proposed that the waves can also induce mixing through transport effects related to the non-conservation of entropy. He considered a turbulent flow described by the largest eddies of sizes at the scale of mixing length which ex-

cites monochromatic oscillation in the radiation zone. In the presence of thermal diffusion, the fluid elements undergo irreversible oscillations due to the loss of entropy and fail to return to their original position, resulting in a mean squared displacement. By relating this displacement to the wave-induced velocity, he derived a diffusion coefficient with a fourth order dependence on wave amplitude, for wave mixing associated with the resulting Stokes displacement. This contrasts with the second order dependence proposed for the wave-induced shear mixing by R. J. Garcia Lopez & H. C. Spruit (1991). Following the work of W. H. Press (1981), later studies improved this approach by incorporating a turbulent spectrum with Kolmogorov scaling, considering a superposition of monochromatic waves excited at the convective radiative interface and modeling the wave excitation by convective plumes rather than by convective eddies that follow the mixing length theory (MLT). These models have been used to explain the Li depletion in solar-type stars (E. Schatzman 1993; J. Montalban 1994; J. Montalban & E. Schatzman 1996; J. Montalbán & E. Schatzman 2000). Taking into account these two distinct mechanisms of wave-induced mixing, P. A. Denissenkov & C. A. Tout (2003) demonstrated that wave mixing by either of these mechanisms could be an additional source of mixing in AGB stars.

Building on these theoretical works, multidimensional hydrodynamic simulations have explored the excitation and propagation of waves in both solar type and massive stars (T. M. Rogers & G. A. Glatzmaier 2005; T. M. Rogers et al. 2013; L. Alvan et al. 2014; L.-A. Couston et al. 2018; P. V. F. Edelmann et al. 2019; R. P. Ratnasingam et al. 2020; S. N. Breton et al. 2022; F. Herwig et al. 2023; J. Morton et al. 2025). Numerical studies have further investigated the transport of angular momentum by these waves (T. M. Rogers & G. A. Glatzmaier 2006; A. J. Barker & G. I. Ogilvie 2010; T. M. Rogers et al. 2013; T. M. Rogers & R. P. Ratnasingam 2025) and have successfully explained the asteroseismically inferred internal rotation rates (T. M. Rogers 2015; C. Aerts 2021). The wave amplitude spectra predictions from the numerical simulations (T. M. Rogers et al. 2013; P. V. F. Edelmann et al. 2019) were also found to be consistent with the observed brightness variation in O and B type stars (C. Aerts & T. M. Rogers 2015; D. M. Bowman et al. 2019).

Such simulations have also been used to investigate chemical mixing by IGWs following different approaches for obtaining the diffusion coefficient. Based on the 3D hydrodynamic simulation of a $25 M_\odot$, F. Herwig et al. (2023) determines a diffusion coefficient in 1D by solving an inverted diffusion equation using a radial profile of the composition as the input (S. Jones et al. 2017). T. M. Rogers & J. N. McElwaine (2017) conducted 2D hydrodynamical simulations of an intermediate mass star with a convective core and radiative envelope and introduced tracer particles in their simulations considering an equatorial geometry. By tracking the trajectories of these particles, they determined the mean squared displacement and the diffusion coefficient for wave mixing. Following their work, A. Varghese et al. (2023) extended the analysis across age and mass. These simulations shows the variation of mixing profile across the radius in the stellar interior and also provided a theoretical prescription based on their findings across different masses and ages. J. S. G. Mombarg et al. (2025) studied the evolution of the Nitrogen surface abundance ratio (I. Hunter et al. 2009; F. Martins et al. 2024) by implementing this mixing prescription in the one dimensional stellar evolution code MESA (B. Paxton et al. 2011, 2013, 2015, 2018, 2019).

The next important step is to gain insight into the dominant physical mechanism responsible for the wave mixing. While T. M. Rogers & J. N. McElwaine (2017) found empirically that the wave mixing was proportional to the wave amplitude squared, they did not link that to any previous theory. F. Herwig et al. (2023) attempted to determine if the mixing caused by IGWs arises from the wave-induced shear instabilities (R. J. Garcia Lopez & H. C. Spruit 1991; J. P. Zahn 1992) and found that the measured mixing by IGWs did not agree with the shear mixing predictions. More recently, J. Morton et al. (2025) investigated the different wave mixing mechanisms proposed by R. J. Garcia Lopez & H. C. Spruit (1991) and W. H. Press (1981) by conducting fully compressible 2D hydrodynamical simulations considering $20 M_\odot$ main sequence star assuming a meridional geometry. They too found that their simulation results did not match either theory, though the R. J. Garcia Lopez & H. C. Spruit (1991) theory had a very similar radial profile. Notably, both the simulations of F. Herwig et al. (2023) and J. Morton et al. (2025) use an implicit large eddy simulation (ILES) approach and while they explicitly set their thermal diffusion coefficients, it is very likely that those values are not accurate and that the thermal diffusion of the simulation is numerical, similar to their viscosity. This is discussed at length in F. Herwig et al. (2023), therefore estimating the actual thermal diffusion to use in making these direct comparisons is somewhat fraught. Moreover, the comparison made by J. Morton et al. (2025) only included one frequency when comparing to and examined theories for diffusion, propagation and generation, making

it difficult to isolate which theory was not in agreement with simulations.[1]

In this work we aim to compare the theoretical prescriptions for wave-induced shear mixing proposed by R. J. Garcia Lopez & H. C. Spruit (1991) and J. P. Zahn (1992) with the diffusion coefficients retrieved in T. M. Rogers & J. N. McElwaine (2017) and A. Varghese et al. (2023) using tracer particles combined with 2D hydrodynamical equatorial simulations. We explicitly isolate the theory for diffusion. Section 2 will discuss the theoretical prescriptions proposed by R. J. Garcia Lopez & H. C. Spruit (1991) and J. P. Zahn (1992). Section 3 will discuss the numerical simulation profiles used in this study. Comparison of these mixing profiles from the numerical studies with the theoretical prescriptions are presented in Section 4 and a detailed discussion on the findings and conclusions are presented in Section 5.

## 2. THEORETICAL PRESCRIPTIONS

### 2.1. *Mixing by wave-induced Shear (R. J. Garcia Lopez & H. C. Spruit 1991; J. P. Zahn 1992).*

A steady flow with sinusoidally varying vertical shear produces small scale turbulence (J. P. Zahn 1975). In a stably stratified region, vertical mixing occurs when the shear is strong enough to overcome the stabilizing effect of the buoyancy in the vertical direction. A flow is said to be unstable when the Richardson number, $Ri$, that compares the effect of the buoyancy force with that of the strength of the shear is less than $1/4$; the Richardson number is defined as:

$$R_i = \frac{N^2}{(\partial u_h/\partial z)^2} \qquad (1)$$

where $N$ is the Brunt-Väisälä frequency, $u_h$ is the horizontal velocity and $z$ is the vertical distance. However, the above is valid only in the absence of thermal diffusion. Thermal diffusion reduces the stabilizing effect of stratification by weakening the restoring force. A. A. Townsend (1958) pointed out that when the thermal timescale, $\tau_t = l^2/K$, of the turbulent element is shorter than its turnover time, $\tau_{ov} = l/v$, where $l$ is the size of the fluid element, $v$ is the velocity of the fluid element and $K$ is the thermal diffusivity, the criterion for instability is modified to:

$$\frac{N^2}{(\partial u_h/\partial z)^2} \frac{\tau_t}{\tau_{ov}} \le \frac{1}{4}. \qquad (2)$$

Building on this understanding of how thermal diffusion influences the shear stability, J. P. Zahn (1992) determined the vertical diffusion coefficient due to turbulent motion. In the presence of a strong horizontal turbulence, the transport of chemicals in the vertical direction triggered by the vertical shear instabilities and meridional flows behaves as a diffusive process (B. Chaboyer & J. P. Zahn 1992). The turbulent motions are stronger in the horizontal direction than in the vertical direction since the latter is inhibited by the buoyant forces (J. P. Zahn 1983). Assuming that the vertical transport is dominated by the largest turbulent eddies that satisfy the modified Richardson criterion for shear instability, J. P. Zahn (1992) proposed the diffusion coefficient associated with turbulence generated by vertical shear as

$$D_{zahn} = \mathcal{C} \left(\frac{du_h}{dr}\right)^2 \frac{K}{N^2}, \qquad (3)$$

where the exact value of $\mathcal{C}$ is unknown and the thermal diffusivity, $K$, is defined as

$$K = \frac{16}{3} \frac{\sigma T^3}{\kappa \rho^2 c_p}. \qquad (4)$$

Assuming that the wave mixing is due to the wave-induced vertical shear and the parameter $\mathcal{C} \sim 0.1$ as determined from the hydrodynamic simulations of V. Prat et al. (2016), we compute the local wave diffusion coefficient based on the above equation in section 4.

R. J. Garcia Lopez & H. C. Spruit (1991) noted that the horizontal oscillation of gravity waves creates a sinusoidally varying vertical shear which can lead to weak turbulence. Accounting for the energy losses by waves due to the work done by the weak turbulence against stable stratification, along with the radiative damping and assuming that the mixing occurs on scales where Eqn. (2) is satisfied, R. J. Garcia Lopez & H. C. Spruit (1991) proposed a diffusion coefficient[2] for the wave-induced mixing,

$$D_{GLS} = \frac{K}{4N^2}(k_v u_h)^2, \qquad (5)$$

where $k_v$ is the vertical wavenumber.

R. J. Garcia Lopez & H. C. Spruit (1991) considered the following inequality

$$k_v u_h > \omega \qquad (6)$$

as a sufficient requirement for their proposed weak mixing mechanism, noting that this criterion must be satisfied for the shear flow produced by IGWs of frequency $\omega$

---

[1] We note that the "clumping" problem for particle tracking seen in J. Morton et al. (2025) does *not* occur in our simulations. We expect that this behavior is due to small-scale discontinuities due to their numerical method (see Appendix A).

[2] Note the equivalence of Eqn. 5 with Eqn. 3 in the case of low-frequency IGWs for which $|d/dr| \sim k_v$ (see S. Mathis 2005).
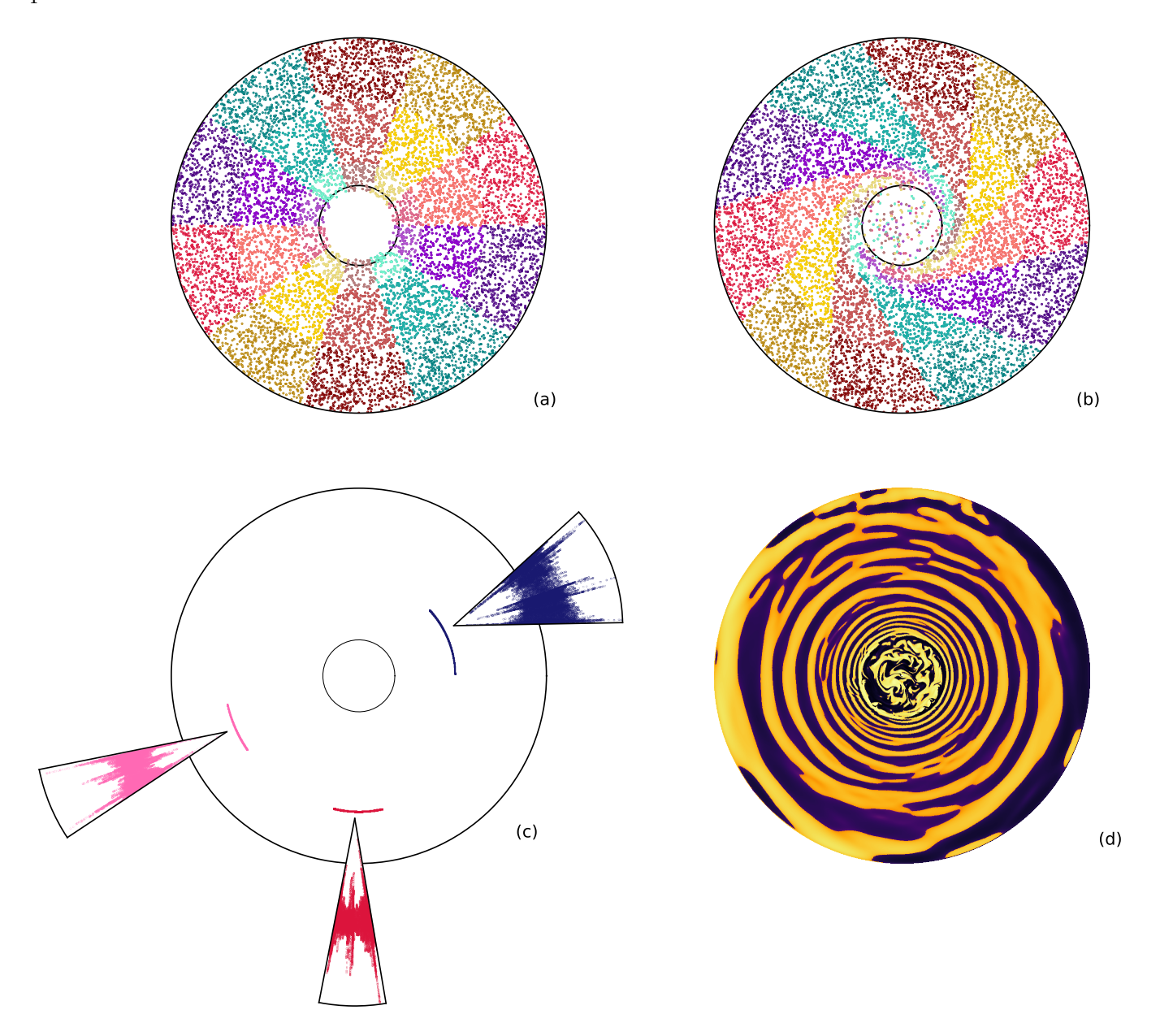
**Figure 1.** (a) Initial and (b) final particle distribution from the tracer particle simulations. The color scheme is chosen to visualize the particle motion with time. (c) The trajectory of a single particle over the whole simulation domain at $0.5R_\star$ (blue), $0.72R_\star$ (red)and $0.7R_\star$ (pink). (d) Vorticity from the 2D simulations with positive vorticity (yellow) saturated at $1\times 10^{-4}$ s$^{-1}$ and negative vorticity (blue) saturated at $-1\times 10^{-4}$ s$^{-1}$. This is for the $7M_\odot$ ZAMS model from A. Varghese et al. (2023).

to be treated as approximately steady state[3]. However, R. J. Garcia Lopez & H. C. Spruit (1991) explicitly note that mixing at lower shear rates was conceivable.

We employ the above two approaches to estimate the diffusion coefficient. The prescription by J. P. Zahn (1992) uses the horizontal velocity directly from the simulation. In contrast, R. J. Garcia Lopez & H. C. Spruit (1991) focus on the wave contribution by decomposing the velocity into frequency and wavenumber components using a Fourier transform. While the underlying form of the equation is the same in both cases, the latter approach specifically targets the wave-driven component of the flow and implicitly includes a time average over the simulation time.

---

[3] Note that Eqn. 6 is equivalent to the breaking criterion proposed by W. H. Press (1981) and derived by S. Mathis (2025).

## 3. MIXING PROFILES FROM 2D HYDRODYNAMICS AND TRACER PARTICLE SIMULATIONS

For the comparison of the theoretical prescription with the simulations, we use the diffusion profiles presented in A. Varghese et al. (2023) for 3, 7 and 20 M$_\odot$ at ZAMS and midMS. The simulations use the background reference state models from MESA and were run for a total simulation time of $\sim 3\times10^7$s considering constant thermal ($\kappa$) and viscous ($\nu$) diffusivities (see Table 1 in Appendix A). These profiles are compared with the theoretical prescriptions discussed in section 2. Figure 1 (a) and (b) shows the initial and final particle distributions from the tracer particle simulation. The trajectory traversed by the particle over the whole simulation time at three different radius is shown in (c) and the vorticity[4] from the 2D simulations is shown in (d). The figure shows a 7M$_\odot$ ZAMS model representing the same simulations from A. Varghese et al. (2023).

## 4. COMPARISON OF THE THEORY WITH THAT OF THE SIMULATION

### 4.1. *Wave-Induced shear mixing*

We initially calculated the local diffusion coefficient based on J. P. Zahn (1992), using Eqn. (3) at a given time and along different horizontal directions. This is shown in Fig. 2 (blue) for a particular horizontal direction. On comparison with that of the simulation profiles (black), we find that these theoretical profiles follow a similar trend as that of the simulation diffusion profiles. We note that the periodic decrease in amplitude occurs when the shear of the wave, i.e., the radial derivative of the horizontal velocity goes to zero. Although this is at one time snapshot and horizontal direction, we found that this agreement is similar for all times and horizontal locations.

We then calculated the diffusion coefficient proposed by R. J. Garcia Lopez & H. C. Spruit (1991) based on the wave-induced vertical shear turbulence, using the Eqn. (5) for frequencies in the range of 3 – 13 µHz and wavenumber, $l = 1$. To obtain the wave velocities, we decomposed the horizontal velocity from the simulation into its frequency and wavenumber components using a Fourier transform in space and time. The range of frequencies and wavenumber were chosen based on the dominant frequencies determined by A. Varghese et al. (2023). We determined the contribution of individual frequencies to the diffusion coefficient and summed over frequencies to retrieve the "GLS" diffusion coefficient, D$_{GLS-sum}$,

$$D_{GLS-sum}(r) = \frac{K}{4N^2} \sum_{\nu=3}^{13\mu Hz} (k_v u_h(r,\omega,m))^2, \quad (7)$$

shown in red in Figure 2. We found that this profile gives us a reasonable agreement between the theory [5] and the simulations . We chose this wavenumber and frequency range as we found these to provide the dominant contribution to mixing in A. Varghese et al. (2023). Moreover, summing over a broader range of frequencies and wavenumbers did not significantly alter the amplitude of the profile. In both cases, we see that the theories from J. P. Zahn (1992) and R. J. Garcia Lopez & H. C. Spruit (1991) give similar results, which is expected since R. J. Garcia Lopez & H. C. Spruit (1991) represents effectively the time average of J. P. Zahn (1992) for low-frequency progressive IGWs. The theoretical diffusion coefficient calculated using Eqn. (7), but with the thermal diffusivities determined by MESA are shown in orange in Fig. 2. This will be discussed further in section 4.2. The green dashed lines in Fig. 2 is based on the study of L. Cope et al. (2020) and will be discussed in detail in Section 5.

### 4.2. *Significance for Observations*

Gaining an understanding of the physical mechanism driving the wave mixing is a major step towards the improvement of stellar evolution models. Recently, J. S. G. Momberg et al. (2025) implemented the wave mixing in the 1D stellar evolution model, MESA. They followed the parameterization proposed by T. M. Rogers & J. N. McElwaine (2017) for the diffusion coefficient as

$$D = Av_{wave}^2, \quad (8)$$

where 'A' is an unknown parameter speculated to depend on various factors, including thermal diffusivity. Their study calibrated this parameter and found that 'A' must increase with stellar mass in order to reproduce the observed nitrogen abundances.

The agreement between theory and simulation presented in this work provides insight into the value of the parameter 'A'. Comparing Eqn. (8) with Eqn. (5), 'A' could be written as ,

$$A \sim \frac{Kk_v^2}{4N^2} \quad (9)$$

which is dependent on the thermal diffusivity. Fig. 3 shows the radial profile of 'A' calculated using this relation but with realistic thermal diffusivity values from

---

[4] Vorticity is defined as $\nabla \times \vec{v}$, where $\vec{v}$ is the fluid velocity.

[5] In the GLS prescription, the periodic decrease of the diffusion coefficient occurs when the horizontal velocity itself changes sign.
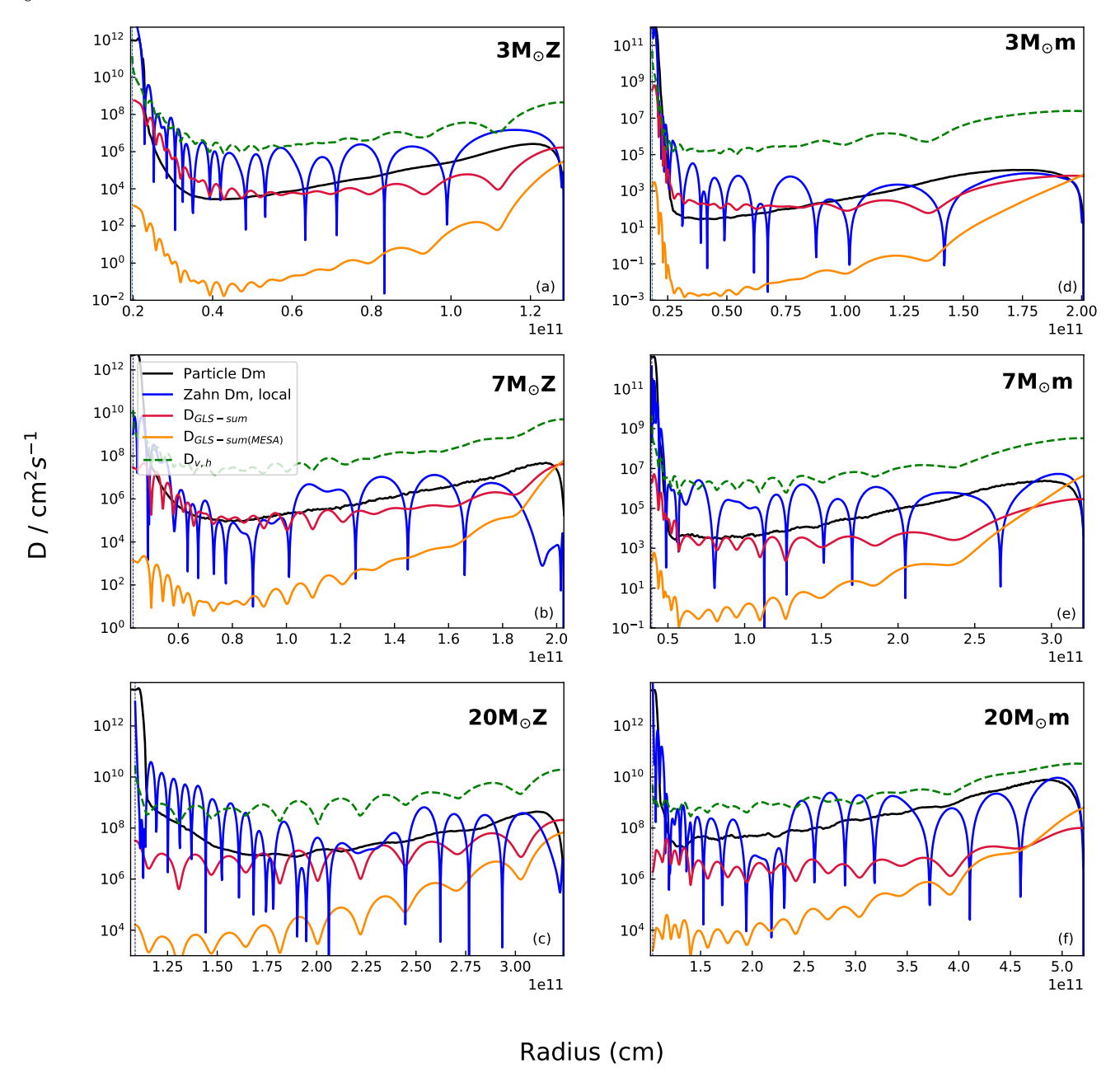
**Figure 2.** Diffusion coefficient from the tracer particle simulation (black) along with the theoretical profiles calculated using Eqn. (3) based on J. P. Zahn (1992) (blue) and Eqn. (5) based on R. J. Garcia Lopez & H. C. Spruit (1991) (red) using the horizontal velocity ($u_h$) from the simulation as a function of radius for $3M_\odot$ (top), $7M_\odot$(middle) and $20M_\odot$ (bottom) for the ZAMS models (left, represented with 'Z') and midMS models (right, represented with 'm'). The diffusion coefficeint calculated from Eqn. (5) but considering realisitic thermal diffusivities from MESA is shown in orange. The green dashed line ($D_{v,h}$) is based on Eqn. (10).

MESA instead of the constant (higher) values used in simulations. The frequencies chosen correspond to the dominant frequencies determined in A. Varghese et al. (2023). We find that 'A' increases with stellar mass, consistent with the trend predicted by the observations (J. S. G. Mombarg et al. 2025). This allows the direct computation of 'A' for implementing wave mixing

in stellar evolution models, taking in to account the underlying physical mechanism.

However, the amplitude of the diffusion coefficient obtained from the simulation also depends on the wave velocity squared and the wave velocity depends on both the convective velocity *and* the thermal and viscous diffusivities in the simulations. Accounting for the convective velocity is straight forward. Our velocities are
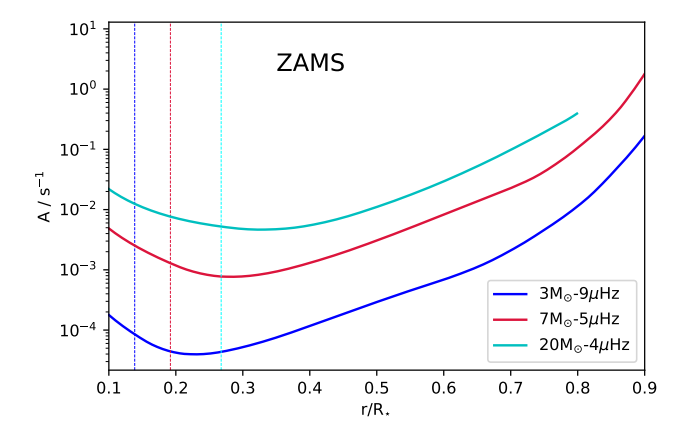
**Figure 3.** The parameter 'A' calculated across masses using Eqn. (9) as a function of fractional radius.

typically 5-15 times larger than MLT and hence, **if** that convective velocity is transferred directly to wave velocity, our diffusion coefficient might be 25-100 times larger than in the actual star. However, there are numerous uncertainties in MLT velocities (M. Joyce & J. Tayar 2023). Moreover, accounting for the effect of enhanced diffusivities on the wave amplitudes is non-trivial. First, these enhanced numerical diffusivities contribute to a larger drop in velocity across the convective-radiative interface than would be expected in an actual star. Second, once convective perturbations transition to waves, the larger thermal and viscous diffusion will damp different frequency waves differently. In both cases the enhanced numerical thermal and viscous dissipation damp low frequencies more, hence reducing their amplitudes and contribution to the measured diffusion coefficient near the convective boundary. On the other hand, thermal and viscous diffusions have little impact on frequencies higher than $\sim 10\mu$Hz and hence likely do not affect the measured diffusion coefficient near the stellar surface. This can be observed in Fig. 2, where the profiles using MESA (orange) and the constant (red) thermal diffusivity have a closer agreement near the surface. Taken together, we expect that the diffusion coefficient obtained using the MESA thermal diffusivity (orange profile) measured near the convective-radiative boundary is a lower limit, while that near the surface is likely close to stellar values. Despite the limitations with these extrapolations, the diffusion coefficients obtained from our simulations are in the expected range inferred from asteroseismic inferences of $10^2 - 10^6$ cm$^2$ s$^{-1}$ for near-core layers (M. G. Pedersen et al. 2018; C. Aerts & A. Tkachenko 2024; H. E. Brinkman et al. 2025), and around $10^5 - 10^6$ cm$^2$ s$^{-1}$ in the envelope based on surface abundance observations (J. S. G. Mombarg et al.
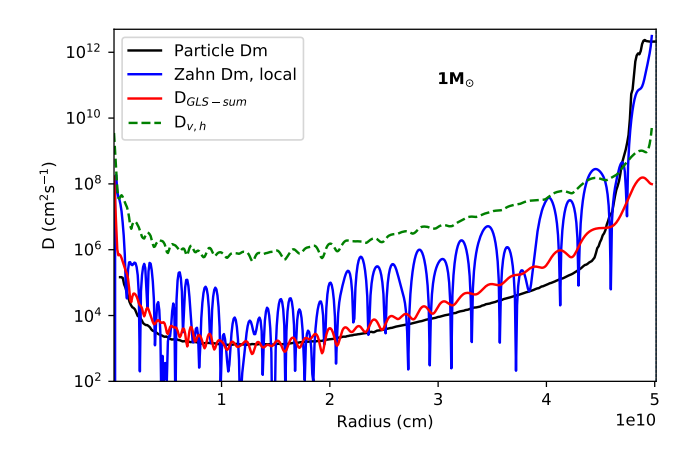


**Figure 4.** Diffusion coefficient from the tracer particle simulation (black) along with the theoretical profiles calculated using Eqn. (3) based on J. P. Zahn (1992) (blue) and Eqn. (5) based on R. J. Garcia Lopez & H. C. Spruit (1991) (red) using the horizontal velocity (u$_h$) from the simulation as a function of radius for 1M$_\odot$ model at solar age. The green dashed (D$_{v,h}$) line is based on Eqn. (10).

2025) and detached eclipsing binaries (H. E. Brinkman et al. 2025).

## 5. DISCUSSIONS AND CONCLUSIONS

The agreement of the theoretical profiles based on R. J. Garcia Lopez & H. C. Spruit (1991)/J. P. Zahn (1992) with the simulation profiles presented in A. Varghese et al. (2023) supports the hypothesis that the underlying mechanism for wave mixing observed in the simulations is due to wave-induced vertical shear. We tested this across a range of simulations, varying mass, age, rotation rate (see Appendix B), convective forcing, thermal diffusion and viscosity and found similar agreement in all cases. Notably, the theoretical predictions also agree well with our recent results of solar type stars with a convective envelope and a radiative core (see Fig. 4). We also highlight that the mixing coefficient near the convective-radiative boundary (at a radius $\sim$ $4.5 \times 10^{10}$ cm) is $\sim 10^4 - 10^6$, which matches the mixing coefficient proposed to explain the Li depletion in the Sun (R. J. Garcia Lopez & H. C. Spruit 1991). The background reference state for the solar models used here are obtained from the 1D stellar evolution code STAREVOL (L. Amard et al. 2016, 2019).

Even though the theoretical prescription of wave-induced shear mixing agrees well with the simulation mixing profiles, the conditions required for developing shear instability, whether based on the criterion from R. J. Garcia Lopez & H. C. Spruit (1991) (Eqn. 6) or the Richardson number being less than 1 (Eqn. 1) are not satisfied everywhere in our simulations. Indeed, if there were an instability, the diffusion coefficients would

be significantly higher and inconsistent with observations. Therefore, we conclude that mixing is instigated by vertical shear but that *weak mixing* does not require instability.

We also extended our comparison to the model proposed by W. H. Press (1981), who derived a diffusion coefficient proportional to $u_h^4$, based on the Stokes displacement, but found that it does not match our simulation profiles (see Fig. 8 in Appendix). We are not testing alternative diffusion due to IGWs breaking (S. Mathis 2025), since we do not observe such phenomena in our simulations.

Turbulent transport in the vertical direction can also arise from 3D motions driven by horizontal shear instabilities (J. P. Zahn 1992; S. Mathis et al. 2018), which may contribute to the observed vertical mixing. This has been numerically tested in several studies (L. Cope et al. 2020; P. Garaud 2020; P. Garaud et al. 2024). L. Cope et al. (2020) found that in thermally diffusive regions, the vertical mixing coefficient can be related to the horizontal turbulence as,

$$D_{v,h} \propto \left( \frac{u_h K}{L_h^3 N^2} \right)^{1/2} u_h L_h \qquad (10)$$

where $L_h$ is of the order of the horizontal wavelength ($\sim k_h^{-1}$). This could possibly explain the presence of vertical transport even when classical vertical shear instability conditions are not satisfied. The above corresponds to a fully 3D configuration, where the radial, latitudinal, and azimuthal directions are all taken into account. In our case, we make use of the fact that, in the theory of linear stellar oscillations, $u_\theta$ and $u_\phi$ are of the same order of magnitude (U. Lee & H. Saio 1997; S. Mathis 2009). We therefore substitute the azimuthal velocity component from our simulation for $u_h$ in Eqn. 10, which should provide the correct order of magnitude. The diffusion profile calculated using Eqn. (10) is shown in Figure 2 (green dotted lines). We observe a similar trend to that of the simulation diffusion profile (black). Although the amplitude differs more than in the profiles obtained using J. P. Zahn (1992) and R. J. Garcia Lopez & H. C. Spruit (1991) prescriptions, the

similar trend supports our argument that wave-driven weak turbulence can cause mixing in stellar interiors.

The overall consistency across different theoretical models and simulations makes weak turbulent mixing a strong candidate. Implementation of these theoretical prescriptions in 1D stellar models can bring us a step closer to calibrating the free parameters in these models using the observational data from the current and upcoming asteroseismic space missions (H. Rauer et al. 2025). However, the fact that the classical Richardson number criterion is not met in these simulations suggests that an additional mechanism may be contributing to the wave-driven mixing. Preliminary work indicates that wave-wave interactions of low-frequency propagating waves with higher frequency standing modes may contribute, but further investigation is required.

# APPENDIX

## A. PARTICLE CLUMPING AND CONVERGENCE OF MIXING PROFILES FROM THE SIMULATIONS

Recently, J. Morton et al. (2025) have raised concern over using tracer particles to measure a diffusion coefficient. This concern is based on particle clumping observed in their simulations (see Figure 9 in that paper). The authors surmise that this issue is due to the particles not following the Eulerian velocity over long time frames. As pointed out by P. P. Popov et al. (2008), S. Genel et al. (2013) and others, this mis-match between Eulerian velocities and particle
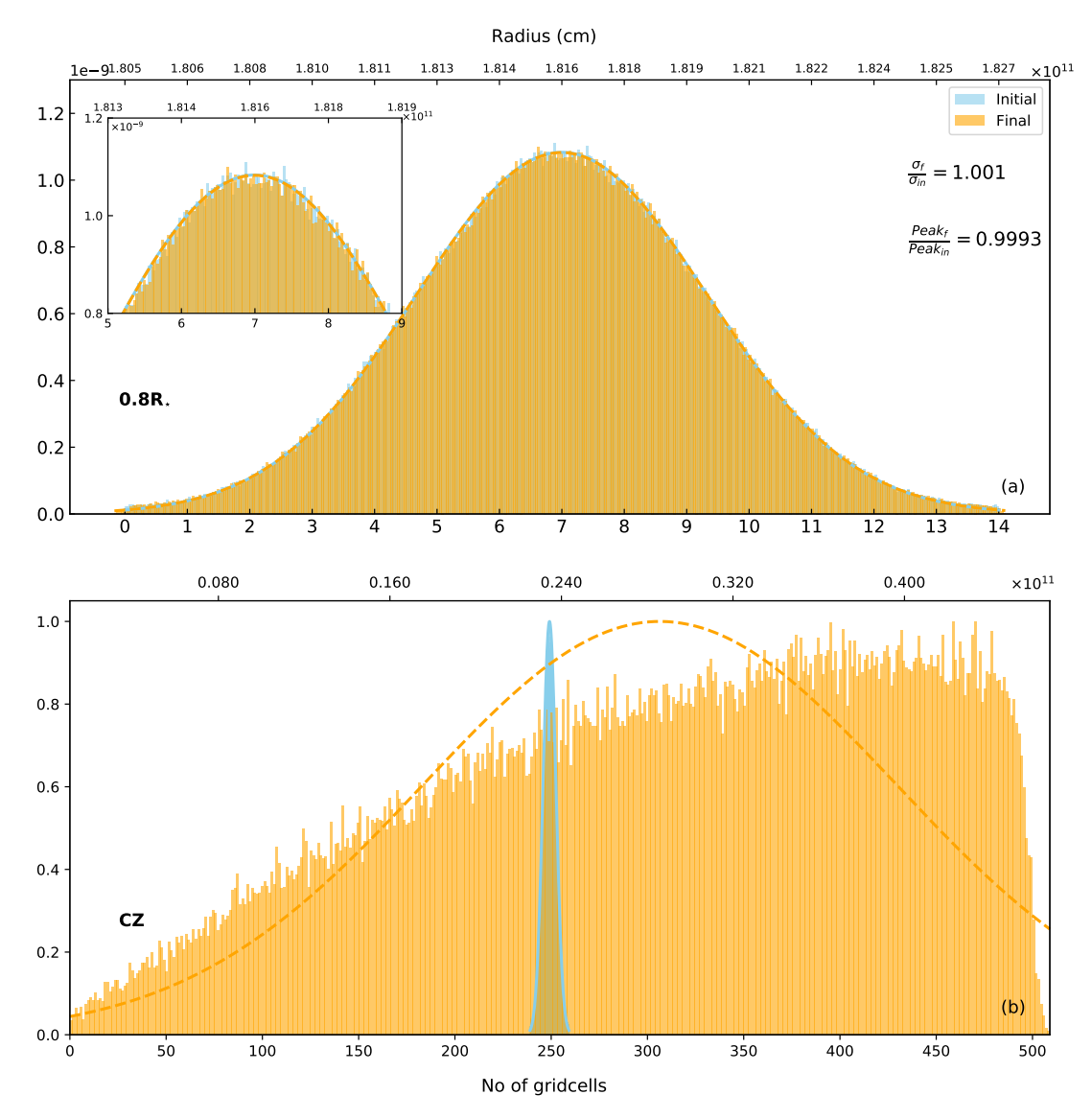
**Figure 5.** Initial (blue) and final (orange) particle distributions for the 7M$_\odot$ ZAMS model as a function of gridcells. (a) Distributions centered around 0.8R$_\star$. The ratio of final-to-initial widths is $\sigma_f/\sigma_{in}=$ 1.001, and the ratio of peak heights is 0.9993. (b) Distributions within the convection zone (cz), normalized for visual comparison. For both panels, the top axis indicates the corresponding stellar radius within which particles are distributed.

(Lagrangian) velocities is most severe at discontinuities in flows (though clumping at cell centers is not typical and indicates a separate problem). To demonstrate that our simulations do not suffer from such numerical artefacts, we repeat the calculation in J. Morton et al. (2025) by initializing particles with a Gaussian distribution centered at 0.8R$_\star$ in our 7M$_\odot$ ZAMS model. Figure 5 (a) shows the initial and final distributions of $10^6$ particles as a function of grid cell and radius. The initial Gaussian profile is preserved at the end of the simulation and no clumping is seen. Though imperceptible on the figure, the Gaussian spreads very slightly over time, consistent with a diffusive behavior. Using the variation in the mean and peak, we calculated the diffusion coefficient directly from the spread of the Gaussian and recover the precise diffusion coefficient at that radius as seen in Figure 2. We note that a Gaussian profile is *not* retained for particles in the convection zone, as expected (Figure 5 (b)).

To demonstrate that the diffusion profiles have converged for all models, we present the radial diffusion profiles at different time differences ($\tau$) for the ZAMS (left) and mid-MS (right) models in Figure 6. The profiles remain essentially unchanged beyond $\tau \sim 2 \times 10^7$ (except for 7 M$_\odot$ ZAMS which required longer time to converge), as seen in the zoomed-in panels for all models. The radial diffusion profile of the 7 M$_\odot$ ZAMS model shown here is an updated
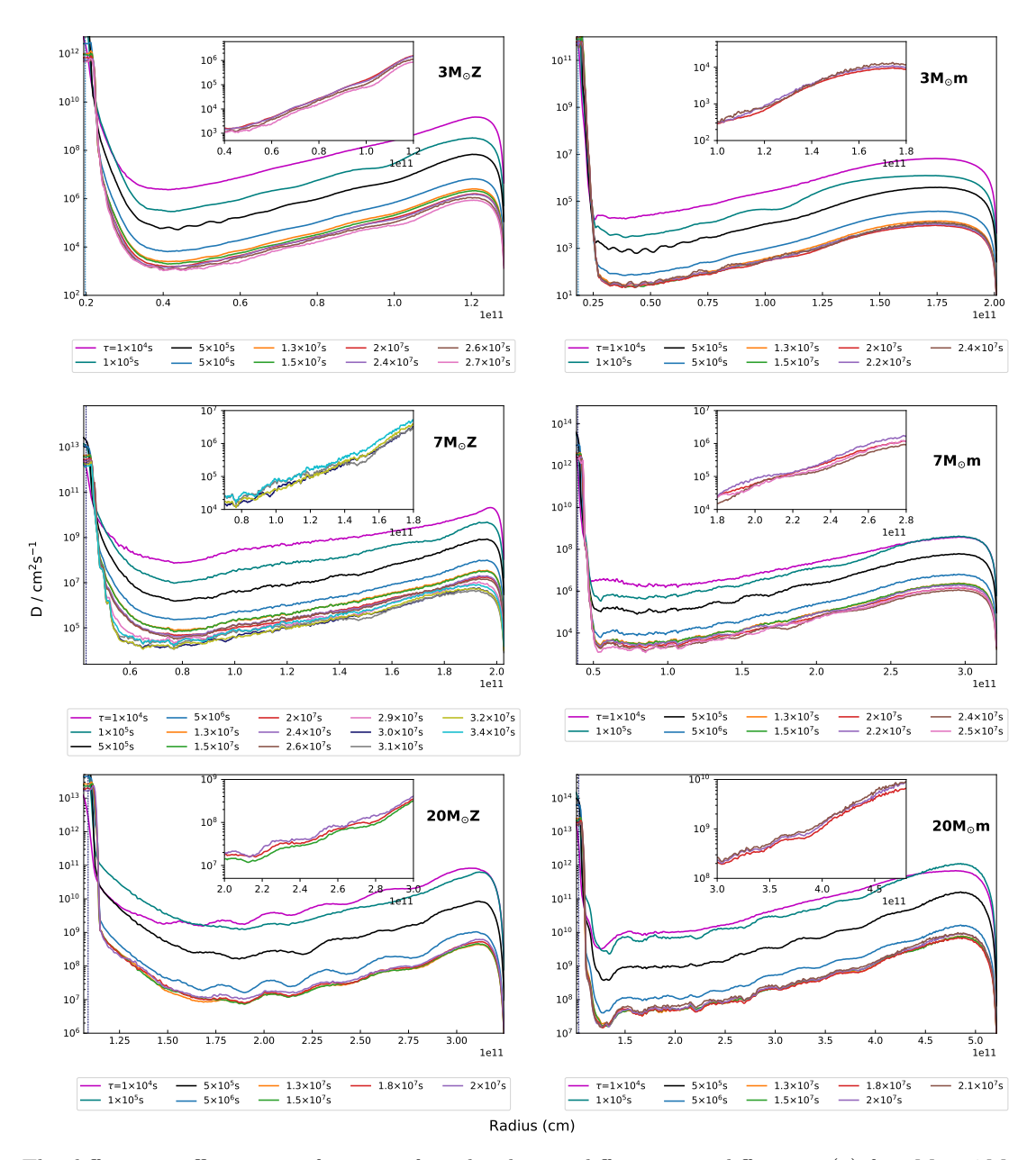
**Figure 6.** The diffusion coefficient as a function of total radius at different time differences ($\tau$) for $3\mathrm{M}_\odot$ , $7\mathrm{M}_\odot$ and $20\mathrm{M}_\odot$ ZAMS (left, represented with 'Z') and midMS (right, represented with 'm') models. The insets highlight the zoomed-in profiles at the latest $\tau$ values.

version of A. Varghese et al. (2023), that was run longer in order to reach equilibrium. Overall, the converged profiles agree well with the prescriptions of R. J. Garcia Lopez & H. C. Spruit (1991) and J. P. Zahn (1992).

We have reproduced the thermal and viscous diffusivities of the models from A. Varghese et al. (2023) in Table 1 for readers' convenience.

### B. COMPARISON OF THE THEORY WITH THAT OF THE SIMULATIONS FOR MODELS WITH DIFFERENT ROTATION RATES

Figure 7 shows the comparison between the diffusion profiles from the numerical simulations of A. Varghese et al. (2024) (black) at different rotation rates ( $\Omega = 1 \times 10^{-5}, 2 \times 10^{-5}, 3 \times 10^{-5}, 4 \times 10^{-5}$ and $1 \times 10^{-4}$ rads$^{-1}$ ) and the mixing profiles computed in this work using the theoretical prescription of J. P. Zahn (1992) (blue) and R. J. Garcia Lopez & H. C. Spruit (1991) (red) for the $7\mathrm{M}_\odot$ midMS model.

| Model | $\kappa, \nu \ / \ 10^{12} \ \mathrm{cm}^2\mathrm{s}^{-1}$ |
|---|---|
| 3M$_\odot$ ZAMS | 5 |
| 3M$_\odot$ midMS | 5 |
| 3M$_\odot$ TAMS | 5 |
| 7M$_\odot$ ZAMS | 5 |
| 7M$_\odot$ midMS | 5 |
| 7M$_\odot$ TAMS | 2.5 |
| 20M$_\odot$ ZAMS | 8 |
| 20M$_\odot$ midMS | 8 |
| 20M$_\odot$ TAMS | 5 |

**Table 1.** Thermal and viscous diffusivities of the models from A. Varghese et al. (2023).

## C. COMPARISON OF WAVE MIXING WITH OTHER THEORETICAL PRESCRIPTIONS

### C.1. *W. H. Press (1981)*

The diffusion coefficient proposed by W. H. Press (1981) taking into account the distance traveled by the fluid element due to the loss of entropy is ,

$$D_{\mathrm{P81}} = \frac{k_h^6 u_h^4 N^2 K^2}{\omega^7}. \tag{C1}$$

We calculated the theoretical diffusion coefficients using Eqn. (C1) across different frequencies for the models presented in this work. Fig. 8 shows the simulation profile in black along with theoretical profile based on W. H. Press (1981) summed over the dominant frequencies (pink). As observed, the amplitude of the profile is $\sim 7 - 8$ orders of magnitude lower than that of the simulation profiles.

## REFERENCES

Aerts, C. 2021, Rev. Mod. Phys., 93, 015001,
doi: 10.1103/RevModPhys.93.015001

Aerts, C., Mathis, S., & Rogers, T. M. 2019, ARA&A, 57,
35, doi: 10.1146/annurev-astro-091918-104359

Aerts, C., & Rogers, T. M. 2015, ApJL, 806, L33,
doi: 10.1088/2041-8205/806/2/L33

Aerts, C., & Tkachenko, A. 2024, Astronomy &
Astrophysics, 692, R1, doi: 10.1051/0004-6361/202348575

Alexander, M. J., Geller, M., McLandress, C., et al. 2010,
Quarterly Journal of the Royal Meteorological Society,
136, 1103, doi: https://doi.org/10.1002/qj.637

Alvan, L., Brun, A. S., & Mathis, S. 2014, A&A, 565, A42,
doi: 10.1051/0004-6361/201323253

Amard, L., Palacios, A., Charbonnel, C., Gallet, F., &
Bouvier, J. 2016, A&A, 587, A105,
doi: 10.1051/0004-6361/201527349

Amard, L., Palacios, A., Charbonnel, C., et al. 2019, A&A,
631, A77, doi: 10.1051/0004-6361/201935160

Barker, A. J., & Ogilvie, G. I. 2010, MNRAS, 404, 1849,
doi: 10.1111/j.1365-2966.2010.16400.x

Bowman, D. M., Burssens, S., Pedersen, M. G., et al. 2019,
Nature Astronomy, 3, 760,
doi: 10.1038/s41550-019-0768-1

Breton, S. N., Brun, A. S., & García, R. A. 2022, A&A,
667, A43, doi: 10.1051/0004-6361/202244247

Brinkman, H. E., Tkachenko, A., & Aerts, C. 2025, arXiv
e-prints, arXiv:2507.20785,
doi: 10.48550/arXiv.2507.20785

Chaboyer, B., & Zahn, J. P. 1992, A&A, 253, 173

Cope, L., Garaud, P., & Caulfield, C. P. 2020, Journal of
Fluid Mechanics, 903, A1, doi: 10.1017/jfm.2020.600

Couston, L.-A., Lecoanet, D., Favier, B., & Le Bars, M.
2018, Journal of Fluid Mechanics, 854, R3,
doi: 10.1017/jfm.2018.669

Denissenkov, P. A., & Tout, C. A. 2003, Monthly Notices of
the Royal Astronomical Society, 340, 722,
doi: 10.1046/j.1365-8711.2003.06284.x

Edelmann, P. V. F., Ratnasingam, R. P., Pedersen, M. G.,
et al. 2019, The Astrophysical Journal, 876, 4,
doi: 10.3847/1538-4357/ab12df

Garaud, P. 2020, ApJ, 901, 146,
doi: 10.3847/1538-4357/ab9c99

Garaud, P., Khan, S., & Brown, J. M. 2024, The
Astrophysical Journal, 961, 220,
doi: 10.3847/1538-4357/ad10b1

Garcia Lopez, R. J., & Spruit, H. C. 1991, ApJ, 377, 268,
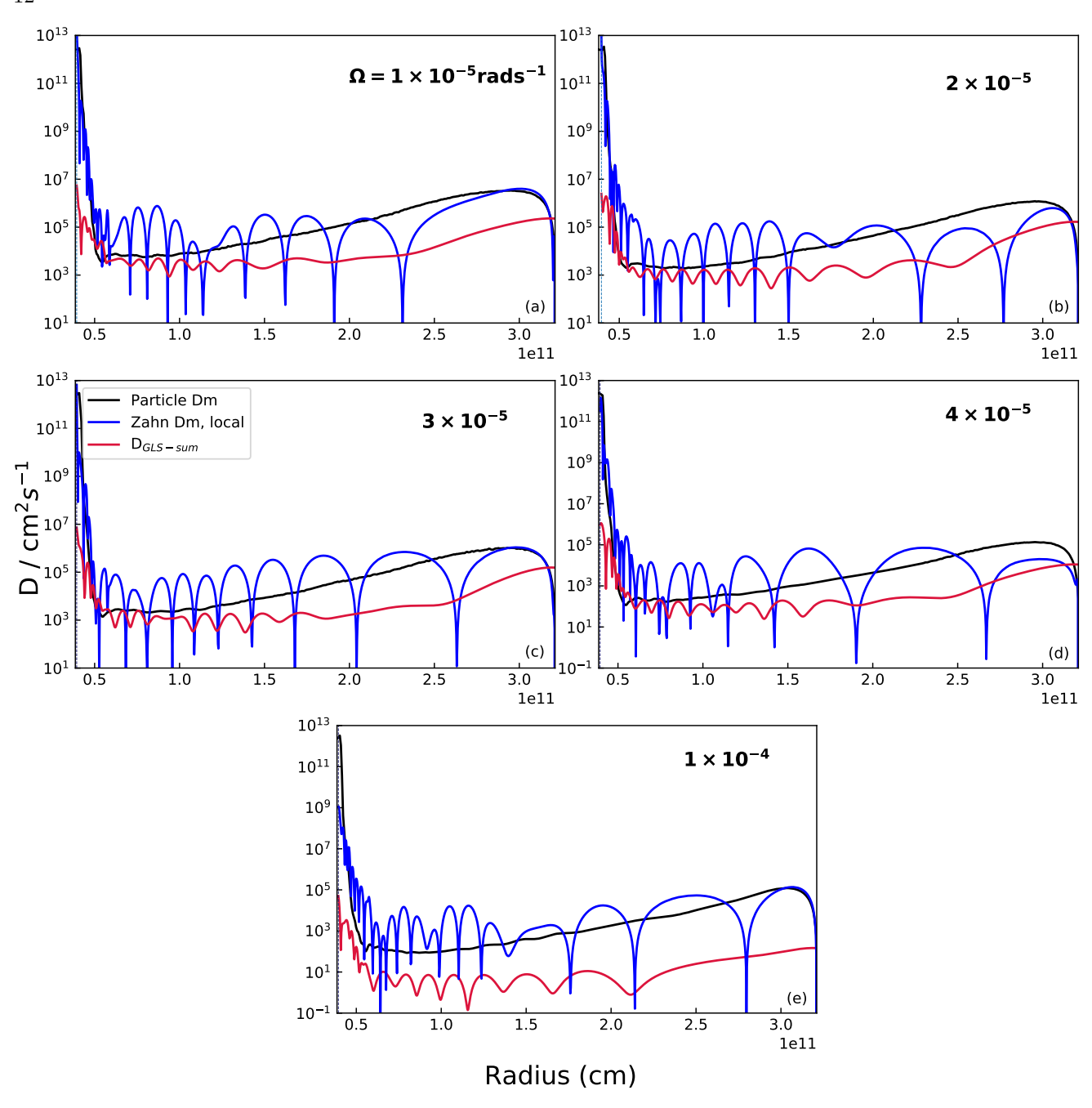doi: 10.1086/170356

**Figure 7.** Diffusion coefficient from the tracer particle simulation (black) along with the theoretical profiles calculated using Eqn. (3) based on J. P. Zahn (1992) (blue) and Eqn. (5) based on R. J. Garcia Lopez & H. C. Spruit (1991) (red) using the horizontal velocity ($u_h$) from the simulation as a function of radius for the $7M_\odot$ midMS model at rotation rates (a) $1 \times 10^{-5}$ (b) $2 \times 10^{-5}$ (c) $3 \times 10^{-5}$ (d) $4 \times 10^{-5}$ and (e) $1 \times 10^{-4}$ rads$^{-1}$ (0.13, 0.27, 0.41, 0.55 and 1.37 d$^{-1}$ respectively).

Genel, S., Vogelsberger, M., Nelson, D., et al. 2013, MNRAS, 435, 1426, doi: 10.1093/mnras/stt1383

Herwig, F., Woodward, P. R., Mao, H., et al. 2023, Monthly Notices of the Royal Astronomical Society, 525, 1601, doi: 10.1093/mnras/stad2157

Holton, J. R. 1982, Journal of Atmospheric Sciences, 39, 791 , doi: 10.1175/1520-0469(1982)039⟨0791: TROGWI⟩2.0.CO;2

Hunter, I., Brott, I., Langer, N., et al. 2009, A&A, 496, 841, doi: 10.1051/0004-6361/200809925

Jones, S., Andrassy, R., Sandalski, S., et al. 2017, MNRAS, 465, 2991, doi: 10.1093/mnras/stw2783

Joyce, M., & Tayar, J. 2023, Galaxies, 11, 75, doi: 10.3390/galaxies11030075

Kumar, P., Talon, S., & Zahn, J.-P. 1999, The Astrophysical Journal, 520, 859, doi: 10.1086/307464
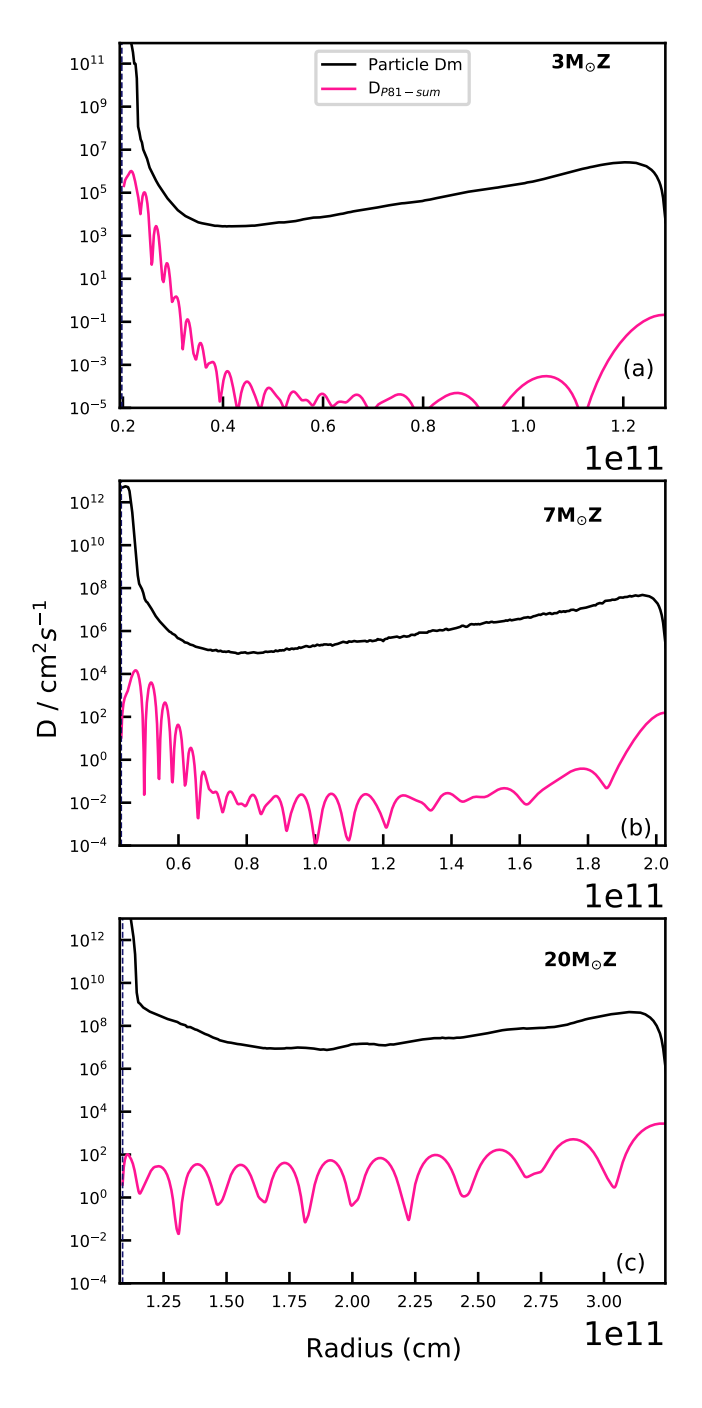
**Figure 8.** The diffusion coefficient from the tracer particle simulation (black) along with the theoretical profile calculated using Eqn. (C1) (pink) using the horizontal velocity ($u_h$) from the simulations for (a) 3M$_\odot$ (b) 7M$_\odot$ and (c) 20M$_\odot$ ZAMS models as a function of radius.

Lee, U., & Saio, H. 1997, ApJ, 491, 839,

doi: 10.1086/304980

Maeder, A. 2009, Physics, Formation and Evolution of Rotating Stars, ed. G. Börner, A. Burkert, W. B. Burton, M. A. Dopita, A. Eckart, T. Encrenaz, E. K. Grebel, B. Leibundgut, A. Maeder, & V. Trimble, Astronomy and Astrophysics Library (Berlin, Heidelberg: Springer Berlin Heidelberg), doi: 10.1007/978-3-540-76949-1

14

Martins, F., Bouret, J. C., Hillier, D. J., et al. 2024, A&A, 689, A31, doi: 10.1051/0004-6361/202449457

Mathis, S. 2005, Phd thesis, Université Paris 11

Mathis, S. 2009, A&A, 506, 811, doi: 10.1051/0004-6361/200810544

Mathis, S. 2013, in Lecture Notes in Physics, Berlin Springer Verlag, ed. M. Goupil, K. Belkacem, C. Neiner, F. Lignières, & J. J. Green, Vol. 865, 23, doi: 10.1007/978-3-642-33380-4_2

Mathis, S. 2025, A&A, 694, A173, doi: 10.1051/0004-6361/202452066

Mathis, S., Prat, V., Amard, L., et al. 2018, A&A, 620, A22, doi: 10.1051/0004-6361/201629187

Mombarg, J. S. G., Varghese, A., & Ratnasingam, R. P. 2025, A&A, 695, A255, doi: 10.1051/0004-6361/202452956

Montalban, J. 1994, A&A, 281, 421

Montalban, J., & Schatzman, E. 1996, A&A, 305, 513

Montalbán, J., & Schatzman, E. 2000, A&A, 354, 943

Morton, J., Guillet, T., Baraffe, I., et al. 2025, MNRAS, 537, 154, doi: 10.1093/mnras/staf010

Paxton, B., Bildsten, L., Dotter, A., et al. 2011, ApJS, 192, 3, doi: 10.1088/0067-0049/192/1/3

Paxton, B., Cantiello, M., Arras, P., et al. 2013, ApJS, 208, 4, doi: 10.1088/0067-0049/208/1/4

Paxton, B., Marchant, P., Schwab, J., et al. 2015, ApJS, 220, 15, doi: 10.1088/0067-0049/220/1/15

Paxton, B., Schwab, J., Bauer, E. B., et al. 2018, ApJS, 234, 34, doi: 10.3847/1538-4365/aaa5a8

Paxton, B., Smolec, R., Schwab, J., et al. 2019, ApJS, 243, 10, doi: 10.3847/1538-4365/ab2241

Pedersen, M. G., Aerts, C., Pápics, P. I., & Rogers, T. M. 2018, A&A, 614, A128, doi: 10.1051/0004-6361/201732317

Popov, P. P., McDermott, R., & Pope, S. B. 2008, Journal of Computational Physics, 227, 8792, doi: 10.1016/j.jcp.2008.06.021

Prat, V., Guilet, J., Viallet, M., & Müller, E. 2016, A&A, 592, A59, doi: 10.1051/0004-6361/201527946

Press, W. H. 1981, ApJ, 245, 286, doi: 10.1086/158809

Ratnasingam, R. P., Edelmann, P. V. F., & Rogers, T. M. 2020, Monthly Notices of the Royal Astronomical Society, 497, 4231, doi: 10.1093/mnras/staa2296

Rauer, H., Aerts, C., Cabrera, J., et al. 2025, Experimental Astronomy, 59, 26, doi: 10.1007/s10686-025-09985-9

Rogers, T. M. 2015, ApJL, 815, L30, doi: 10.1088/2041-8205/815/2/L30

Rogers, T. M., & Glatzmaier, G. A. 2005, Monthly Notices of the Royal Astronomical Society, 364, 1135, doi: 10.1111/j.1365-2966.2005.09659.x

Rogers, T. M., & Glatzmaier, G. A. 2006, ApJ, 653, 756, doi: 10.1086/507259

Rogers, T. M., Lin, D. N. C., McElwaine, J. N., & Lau, H. H. B. 2013, The Astrophysical Journal, 772, 21, doi: 10.1088/0004-637X/772/1/21

Rogers, T. M., & McElwaine, J. N. 2017, ApJL, 848, L1, doi: 10.3847/2041-8213/aa8d13

Rogers, T. M., & Ratnasingam, R. P. 2025, ApJL, 983, L38, doi: 10.3847/2041-8213/adc45a

Schatzman, E. 1993, A&A, 279, 431

Talon, S., & Charbonnel, C. 2005, Astronomy & Astrophysics, 440, 981–994, doi: 10.1051/0004-6361:20053020

Townsend, A. A. 1958, Journal of Fluid Mechanics, 4, 361, doi: 10.1017/S0022112058000501

Varghese, A., Ratnasingam, R. P., Vanon, R., et al. 2024, The Astrophysical Journal, 970, 104, doi: 10.3847/1538-4357/ad54b5

Varghese, A., Ratnasingam, R. P., Vanon, R., Edelmann, P. V. F., & Rogers, T. M. 2023, The Astrophysical Journal, 942, 53, doi: 10.3847/1538-4357/aca092

Zahn, J. P. 1975, Memoires of the Societe Royale des Sciences de Liege, 8, 31

Zahn, J. P. 1983, in Saas-Fee Advanced Course 13: Astrophysical Processes in Upper Main Sequence Stars, ed. A. N. Cox, S. Vauclair, & J. P. Zahn, 253

Zahn, J. P. 1992, A&A, 265, 115

Zahn, J. P., Talon, S., & Matias, J. 1997, A&A, 322, 320. https://arxiv.org/abs/astro-ph/9611189